

Detecting Brain Growth Patterns in Normal Children using Tensor-Based Morphometry

Xue Hua,¹ Alex D. Leow,^{1,2} Jennifer G. Levitt,³ Rochelle Caplan,³
Paul M. Thompson,¹ and Arthur W. Toga^{1*}

¹Laboratory of Neuro Imaging, Brain Mapping Division, Department of Neurology,
University of California Los Angeles School of Medicine, Los Angeles, California

²Resnick Neuropsychiatric Hospital, University of California Los Angeles School of Medicine,
Los Angeles, California

³Department of Psychiatry and Biobehavioral Sciences, Division of Child Psychiatry,
University of California Los Angeles School of Medicine, Los Angeles, California

Abstract: Previous magnetic resonance imaging (MRI)-based volumetric studies have shown age-related increases in the volume of total white matter and decreases in the volume of total gray matter of normal children. Recent adaptations of image analysis strategies enable the detection of human brain growth with improved spatial resolution. In this article, we further explore the spatio-temporal complexity of adolescent brain maturation with tensor-based morphometry. By utilizing a novel non-linear elastic intensity-based registration algorithm on the serial structural MRI scans of 13 healthy children, individual Jacobian growth maps are generated and then registered to a common anatomical space. Statistical analyses reveal significant tissue growth in cerebral white matter, contrasted with gray matter loss in parietal, temporal, and occipital lobe. In addition, a linear regression with age and gender suggests a slowing down of the growth rate in regions with the greatest white matter growth. We demonstrate that a tensor-based Jacobian map is a sensitive and reliable method to detect regional tissue changes during development. *Hum Brain Mapp* 30:209–219, 2009. © 2007 Wiley-Liss, Inc.

Key words: brain development; Jacobian; longitudinal; MRI; nonlinear image registration; TBM

Contract grant sponsor: National Institutes of Health [NIH Roadmap for Medical Research Grant entitled Center for Computational Biology (CCB)]; Contract grant number: U54 RR021813; Contract grant sponsor: National Center for Research Resources (NCRR), National Institutes of Health (NIH); Contract grant numbers: P41 RR013642, M01 RR000865; Contract grant sponsor: National Alliance for Autism Research; Contract grant number: 01082668; Contract grant sponsor: National Institute of Mental Health; Contract grant numbers: 5K08 MH01385, MH067187; Contract grant sponsor: National Institute of Neurological Disorders and Stroke; Contract grant numbers: 5R01 NS046018, NS32070.

*Correspondence to: Arthur W. Toga, Laboratory of Neuro Imaging, Department of Neurology, UCLA School of Medicine, 635 Charles Young Drive South, Suite 225, Los Angeles, CA 90095-7334, USA. E-mail: toga@loni.ucla.edu

Received for publication 15 September 2006; Revised 20 August 2007; Accepted 11 September 2007

DOI: 10.1002/hbm.20498

Published online 6 December 2007 in Wiley InterScience (www.interscience.wiley.com).

INTRODUCTION

Advancements in magnetic resonance imaging (MRI) technology and image analysis methods make the detailed characterization of human brain development during childhood and adolescence *in vivo* possible. The maturation of a normal brain represents a complex and dynamic developmental process. Detailed spatial and temporal mapping of structural changes during this process aids in understanding the basis of age-related cognitive advancement and various brain developmental disorders.

Cross sectional neuroimaging studies have consistently demonstrated reduction in overall cerebral gray matter volume and growth in white matter with relatively stable total brain volume from ages 4 to 20 years [Caviness et al., 1996; Giedd et al., 1996; Jernigan et al., 1991; Pfefferbaum et al., 1994; Reiss et al., 1996; Sowell et al., 1999a]. Fewer studies have used longitudinal data to examine the dynamic patterns of brain growth between childhood and adolescence. Giedd et al. [1999] demonstrated a linear increase in white matter and non-linear changes in gray matter volume in a large-scale longitudinal pediatric neuroimaging study. Thompson et al. [2000] applied a tensor mapping technique to a group of children repeatedly scanned between the ages of 3 and 15 years and found a rostro-caudal wave of growth at the corpus callosum in the developing human brain. Sowell et al. [2004] described correlated changes in cortical thickness and regional brain size in right frontal and bilateral parieto-occipital regions in children scanned twice between the ages of 5 and 11 years. Because the longitudinal method follows the same brain as it matures, it addresses the issue of inter-individual variations in brain structures. As such, it provides a more sensitive and finer toned measurement of individual growth patterns than cross-sectional studies [Chung et al., 2001; Giedd et al., 1999; Hand and Crowder, 1996; Sowell et al., 2004; Thompson et al., 2000].

Studies using MRI-based volumetry have provided a wealth of information for age-related changes in brain morphometry [Giedd et al., 1996; Reiss et al., 1996]. However, traditional MRI-based volumetric methods demand manual or semi-automatic image segmentations of the equivalent regions across multiple brains. Measurements obtained using these methods are usually confined to brain regions that can be clearly defined. More recently, tensor-based morphometry (TBM) has been introduced as a method to identify regional structural differences from the gradients of deformation fields (reviewed in Ashburner and Friston [2003]). A deformation field, which stores the relative positions of different brain structures, is first obtained by spatially normalizing the MRI images of one brain to another using non-linear registration. To characterize local shape differences, a tensor field, also known as a Jacobian matrix, is then calculated from the gradient of the deformation field. A determinant is taken at each point of the Jacobian matrix field to represent the volume of the unit-cube after the deformation. Jacobian determinants are

usually coded by colors to indicate local volume loss or gain [Ashburner and Friston, 2003; Chung et al., 2001; Freeborough and Fox, 1998; Riddle et al., 2004; Toga, 1999]. When the TBM method is applied to longitudinal data, the deformation field is obtained by registering the MRI scans of the same subject acquired at different times. Therefore, the Jacobian map faithfully represents the developmental changes in the brain. Because the Jacobian matrix field is calculated over the entire volume without explicit delineations of regions-of-interest (ROI), the TBM method characterizes the local shape differences with a much higher spatial resolution.

In this article, TBM is used to generate detailed tissue growth maps from the longitudinal scans of 13 healthy children between the ages of 6 and 19 years. By fitting a linear model across all individual Jacobian maps voxel-by-voxel, we also evaluate age and gender-related volume changes in gray and white matter. We create three-dimensional (3D) maps that represent the dynamics of brain development, demonstrating a slowing down of the growth rate over time in regions with the greatest white matter growth.

MATERIALS AND METHODS

Subjects

Thirteen healthy children and adolescents (seven males and six females) aged 6–19 are included in this article (Fig. 1). The mean age for the group was 12.3 ± 2.6 years. Each subject received a series of two high-resolution 3D magnetic resonance imaging (MRI) scans with an average inter-scan interval of 2.85 ± 0.85 years (min = 1.92 years; max = 4.52 years). There was no significant age difference between males (12.3 ± 2.4 years) and females (12.3 ± 2.9 years). All subjects were recruited as part of an ongoing neuro-developmental project at the University of California, Los Angeles (UCLA). The subjects were screened for neurological, psychiatric, language, or hearing disorders by clinical interview, and for developmental history and K-SADS_PL [Kaufman et al., 1997] through interviews with the parents. This study was approved by the UCLA Human Subjects Protection committee and all parents of subjects provided written informed consent for participation.

MRI Acquisition

The sensitivity and reliability of TBM depend on the contrast and stability of the scans. Thus, we followed the standard scanning procedure. All scans were conducted on a GE Signa 1.5 Tesla MRI scanner (GE Medical Systems, Milwaukee, WI). High-resolution 3D MRI scans for each subject were acquired with T1-weighted spoiled GRASS (SPGR) sequences. A sagittal plane imaging acquisition protocol was used with repetition time (TR) of 24 ms, echo time (TE) of 9 ms, and flip angle of 22° , and 2 excitations. The acquisition matrix was $256 \times 256 \times 124$ with slice

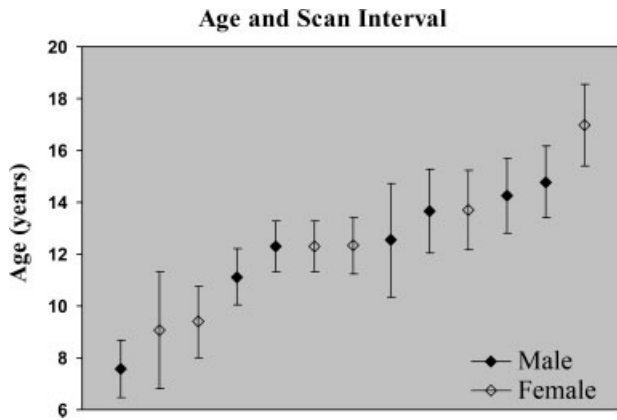


Figure 1.

Ages and inter-scan intervals. Thirteen subjects are included in this study with seven males and six females. The graph shows the subjects' ages (◆ male; ◊ female) and their corresponding inter-scan intervals (vertical bars).

thickness of 1.2 mm and field of view of 24 cm. The image voxel size was $0.9375 \times 0.9375 \times 1.2$ mm.

Image Preprocessing

Skull and other non-brain tissues were removed using an automated program, Brain Surface Extractor (BSE), from the BrainSuite [Shattuck and Leahy, 2002]. A binary mask was generated to include brain tissues like gray matter, white matter, and cerebrospinal fluid. Non-brain tissues (such as skull, scalp, and orbits) were left out and labeled as zero. All sagittal plane images were manually edited to lower the segmentation error caused by similar image intensities between brain and non-brain tissues. A 3D radio frequency (RF) bias field correction algorithm (N3) was applied to eliminate the field inhomogeneity in MRI images caused by non-uniformities in the RF receiver coils [Sled et al., 1998]. A validation study has demonstrated the robustness of TBM with scans acquired using SPGR sequence followed by N3 correction [Leow et al., 2005b].

To account for global differences in positioning and size among individual brains, all scans were rigidly aligned to the stereotactic space defined by the International Consortium for Brain Mapping (ICBM) [Mazziotta et al., 2001]. Specifically, we used the ICBM 53 atlas which is an average of 53 T1-weighted MRI scans of young healthy adult brains. To linearly align the scans to ICBM53, a follow-up scan was linearly registered to its baseline scan with 6-parameter (6p) affine transformation, then both scans were registered to ICBM53 using a same 9-parameter (9p) transformation. Mutual information (MI), a measure of the statistical dependence between two distributions, was used as a similarity measure for the above global transformations [Maes et al., 1997]. At the step of 9p linear registration to

ICBM53, all MRI images were resampled into an isotropic matrix of 199 voxels in x -, y -, and z -dimensions with each voxel interpolated to the size of $1 \text{ mm} \times 1 \text{ mm} \times 1 \text{ mm}$.

To inspect the quality of linear registrations, we used a 3D visualization tool called REGISTER, which automatically overlays the arbitrary slice geometry of each scan pairs in ICBM53 space [MacDonald, 1993]. All scans had satisfactory results for linear registration without noticeable distortion or mismatch.

Minimal Deformation Target

Studies have suggested that registration bias can be reduced by using an unbiased group-average template. We therefore constructed a minimal deformation target (MDT) [Good et al., 2001; Kochunov et al., 2002; Kovacevic et al., 2005; Woods et al., 1998]. To compute a MDT, the first step was to create an affine average. All baseline images were registered to ICBM53 using 9-parameter affine transformations. After intensity normalization, the affine average template was created by calculating the mean intensity at each voxel of the 13 scans. The second step was to create a non-linear average. Here, each scan was non-linearly registered to the affine average template using a non-linear inverse consistent elastic intensity-based registration algorithm [Leow et al., 2005a,b; Thompson et al., 2000; Wells et al., 1996]. The deformation field was determined by maximizing the mutual information of the image intensities and minimizing the elastic energy of the deformation. A multi-resolution scheme was used. It started with a Fast Fourier Transform (FFT) resolution of $32 \times 32 \times 32$ and was followed by $64 \times 64 \times 64$, which corresponds to an effective voxel size of 30 mm^3 ($199 \text{ mm}/64 = 3.1 \text{ mm}$). Convergence of MI was achieved iteratively with 300 iterations at each resolution. We then created the non-linear average brain by voxel-wise averaging the intensities of the 13 images that have been non-linearly registered to the affine average template. Finally, we created the MDT by adjusting the non-linear average with inverse geometric

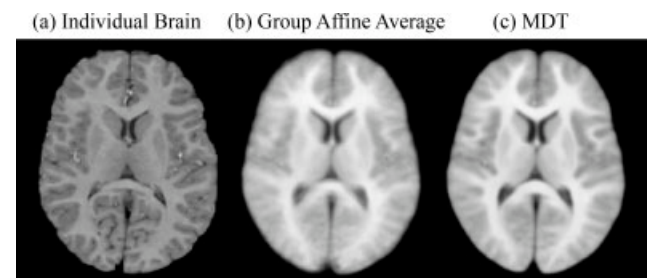


Figure 2.

Minimal deformation target (MDT). The figure displays an axial slice ($z = 112$) from (a) a randomly selected individual brain (b) group affine average and (c) MDT. MDT is an unbiased brain template that represents the common anatomy and anatomical variations within the group.

centering of the displacement fields [Kochunov, et al., 2002, 2005]. The MDT was subsequently used as the target for inter-subject registration. Figure 2 displays the axial slice of a randomly chosen individual brain, the group affine average, and the MDT. The MDT reveals less anatomical detail than the individual brain but it has less noise and higher contrast compared to the affine average.

Jacobian Maps Construction

The same non-linear registration algorithm as used in MDT construction was also used here to spatially normalize both intra- and inter-subject shape differences. The deformation field obtained from intra-subject scan pairs U_{Intra}^n (n : subject index) represents individual growth (Fig. 3). Annualized tissue change maps were derived from the deformation field obtained by warping the follow-up scan of each subject to its baseline scan. Fifty iterations were computed at each FFT resolution. The inter-subject registration U_{Inter}^n encodes the variance between individual brain anatomies. To conform individual Jacobian maps to the same stereotactic space, the initial scan of each subject

was non-linearly aligned to the geometry of the MDT template ($32 \text{ FFT} \times 300$ iterations; $64 \text{ FFT} \times 300$ iterations). The inter-subject displacement vector field $U_{\text{Inter}}^n = (u_x, u_y, u_z)$, obtained from this step, was then applied to transform the Jacobian growth map of each subject to the brain coordinate defined by the MDT. Spatial normalizations among different brains enable regional comparisons and group analyses to be performed. See Figure 4 for a diagram of the design. This approach is computationally intensive; however, it helps to lower the vast inter-individual variance in brain anatomy.

To adjust for variable time differences between scans, we normalized the individual Jacobian maps by their inter-scan intervals. As such, each map (percent tissue change) was divided by its corresponding inter-scan interval to create the annualized Jacobian map, which represents the average change over 1 year. All results and statistical analyses are based on the annualized Jacobian maps.

All image processing steps were automated using LONI Pipeline Processing Environment which streamlines the process and allows parallelization of multiple tasks [Rex et al., 2003].

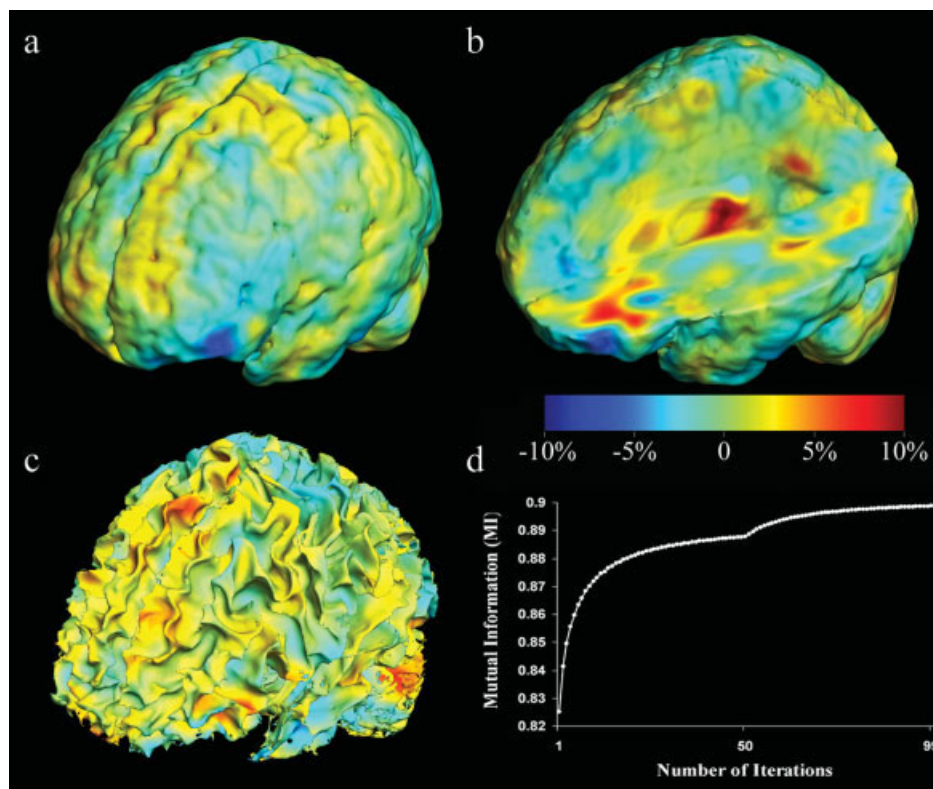


Figure 3.

Individual Jacobian (growth) map. The annualized Jacobian map, representing the percentage of tissue growth per year, of an 8-year-old boy, is displayed on cortical surface model (a), a cortical model with the medial surface exposed (b), and white matter

surface model (c). (d) plots the MI values versus the number of iterations. The transient increase in MI value after the 50th iteration is caused by up-sampling of the FFT resolution from 32×32 to $64 \times 64 \times 64$.

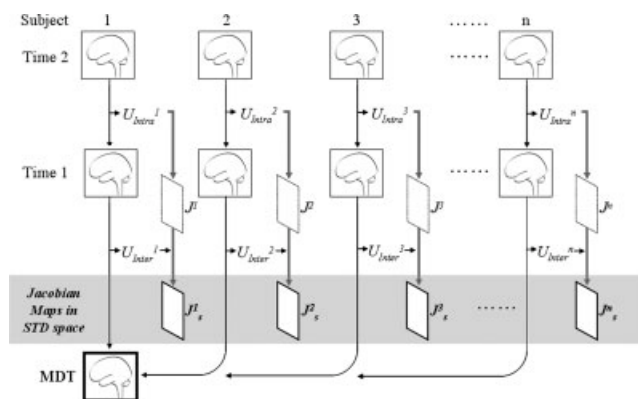


Figure 4.

Warp diagram. Individual Jacobian maps are derived from the deformation matrix U_{intra}^n , which is obtained by iteratively deforming the follow-up scan (Time 2) to the initial scan (Time 1) of the same subject. Variance between individual brains is explained by inter-subject registration, U_{inter}^n . The displacement vector field $U_{inter}^n = (u_x, u_y, u_z)$ is applied to transform the Jacobian growth map of each subject (J^n) to the brain anatomy defined by the MDT template (bolded border). J_s^n represents the individual Jacobian map in the standard space.

Regions-of-Interest

ROI were defined according to the group average in the ICBM53 space. Each brain was hand-traced by a trained anatomist to generate masks that cover frontal, parietal, temporal, and occipital regions separately. The masks were then transformed into the ICBM space and the mathematical average of the masks was used to estimate the probabilities of each region-of-interest. Brain regions were defined based on probabilities that are greater than 70%.

Statistical Analyses

To assess the significance level of the Jacobian maps at each voxel, we applied the bootstrap method [Efron and Tibshirani, 1986, 1993]. Specifically, we generated 1,000 independent bootstrap samples, each of size $n = 13$ with replacements from the 13 individual Jacobian maps. The bootstrap estimate of standard error is the standard deviation of the bootstrap replications [Efron and Tibshirani, 1993]. At each voxel, a one-sample t -test was conducted based on the bootstrap sample mean and bootstrap esti-

mate of standard error. Next, permutation tests were implemented to correct for multiple comparisons. Permutation tests are non-parametric in nature, and are used in this study to assess the overall significance of Jacobian maps inside each region-of-interest. In our case, the null hypothesis in consideration is that, for each ROI, there is no tissue growth or loss. Under null hypothesis, the labels of time 1 and time 2 are interchangeable within each subject. In other words, we can thus randomly multiply 1 or -1 to the Jacobian map of each subject, as each Jacobian map is simply noise under null. This procedure is, in essence, the same as what was originally proposed by Nichols [Nichols and Holmes, 2002], where group labels were permuted (in our case, the two group labels are time 1 versus time 2). At each permutation, a label of 1 or -1 was randomly assigned to each of the 13 subjects and voxels with $P \leq 0.05$ (uncorrected) were identified. After 10,000 randomized tests, a ratio was calculated describing what fraction of time an effect of similar or greater magnitude to the real effect occurs in the random assignments. This ratio serves as an overall estimate of significance for the maps (corrected for multiple comparisons) [Nichols and Holmes, 2002]. Positive growth signals and negative tissue loss were assessed separately in each region-of-interest (frontal, parietal, temporal, and occipital lobes) (Table I). For example, the permutation test of positive Jacobian values rendered a P -value of 0.0054 (frontal lobe) (Table I), indicating the overall significance level of tissue expansion in the frontal lobe.

Age and gender effects were tested by modeling the data with linear regression:

$$\begin{aligned} \text{annual tissue growth rate} &= \beta \cdot (\text{age} - \text{mean age}) + \alpha \\ \text{annual tissue growth rate} &= \beta \cdot (\text{age} - \text{mean age}) \\ &\quad + (\chi \cdot \text{gender} + \alpha) \end{aligned}$$

The annual tissue growth rate was modeled with a constant term α (intercept) which represents the percentage of annual growth at the mean age, and a linear coefficient β (slope) that encodes the change of growth rate. To compare our result with direct modeling of gray matter volume [Giedd et al., 1999], the intercept α corresponds to the slope of the developmental trajectory of gray matter volume. Likewise, the linear coefficient β is comparable to the quadratic term of gray matter regression. Gender effect was explored by adding an additional term χ , which is a gender specific component of α . Here we assumed that

TABLE I. Permutation test results^a

	Frontal lobe	Parietal lobe	Temporal lobe	Occipital lobe
Tissue expansion ($J > 0$)	0.0054	0.0211	0.0635	0.0111
Tissue shrinkage ($J < 0$)	0.3069	0.0018	0.0211	0.0096

^a The permutation test is not corrected for multiple ROI comparisons. Theoretically, one of the ROIs might be significant by accident. However, the highly significant P values suggest those large effects can hardly be achieved by chance.

males and females share the same slope term β , as developmental curves were found to have similar shapes for both genders [Giedd et al., 1999], therefore the second time derivative of the curves which is also the slope of our linear regression model would be the same. Student's *t*-tests were used to examine the voxel-level significance of the regression coefficients (uncorrected). Permutation tests were used to assess the overall significance of age correlation (ROI—the entire brain). A null distribution was constructed after 10,000 random tests. For each test, the subjects' ages were randomly permuted and voxel-wise regressions were conducted to identify voxels with age correlation coefficient more significant than $P = 0.05$. Similar to the method introduced earlier, a ratio, describing the fraction of time an random effect of similar or greater magnitude to the real effect, was calculated to quantify the overall significance of the age effect (corrected for multiple comparisons) [Chiang et al., 2007; Thompson et al., 2003; Nichols and Holmes, 2002].

RESULTS

Individual Growth Map

To illustrate how this non-linear registration technique provides a detailed depiction of brain development, the individual tissue change map of an 8-year-old boy (initial

scan conducted at age 6) is shown in Figure 3. The annualized Jacobian map is superimposed on gray or white matter surface models (generated using the tissue classification tool in BrainSuite [Shattuck and Leahy, 2002]). The annualized growth rate is displayed in color map with the hot and cold color representing local tissue expansion and atrophy respectively. Correspondingly, we visually inspected all individual Jacobian maps and they share similar features to the individual brain reported in Figure 3. However, older subjects generally display fewer changes with weaker growth signals.

Mean Jacobian Map

Figure 5 displays the annualized mean Jacobian map of the 13 subjects after bootstrap correction. The widespread regions of tissue growth primarily correspond to the anatomical boundaries of cerebral white matter. The volume of fiber tract is also enlarged in several sub-regions of the corpus callosum including genu, isthmus (arrow in Fig. 5), and splenium.

Permutation Tests

Next, permutation tests were conducted to correct for multiple comparisons. The results provide overall significant levels of tissue expansion or atrophy in each region-of-interest. Ten thousand randomization tests were

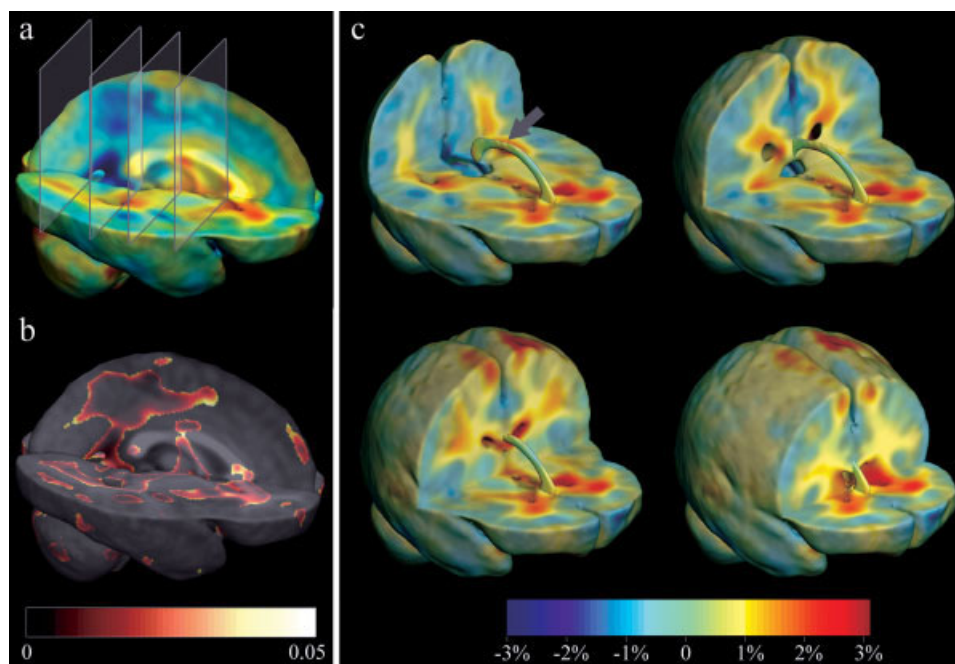


Figure 5.

Group mean growth map with *t* map. The bootstrap corrected mean growth map is computed after all 13 individual maps are geometrically aligned to the standard space. (a) and (b) display the annualized mean growth rate and voxel-wise *t*-test result

($P \leq 0.05$) respectively. Four different coronal sections ($y = 53, 83, 103, \text{ and } 133$) and the corpus callosum are shown in (c). The location of callosum isthmus is indicated by the arrow.

conducted and rendered significant P -values ($P \leq 0.05$) of tissue expansions in the frontal, parietal, and occipital lobes. Concurrently, permutation tests validated the tissue loss in the parietal, temporal and occipital lobes. As shown in the mean map (Fig. 5), the regions of expansion correspond generally to the white matter, while the majority of atrophies are located in the gray matter (except in the primary sensorimotor areas). Thus, the permutation results of tissue expansions correspond mainly to the white matter growth and atrophies are related largely to the gray matter

loss. Refer to Table I for the full results from the permutation tests.

Age and Gender Effects

Age effects in growth patterns are studied by fitting a linear regression model voxel-by-voxel over the Jacobian matrix maps, with Jacobian values as dependent variables and ages as explanatory variables. Figure 6 shows the regression coefficients (terms α and β) and the correspond-

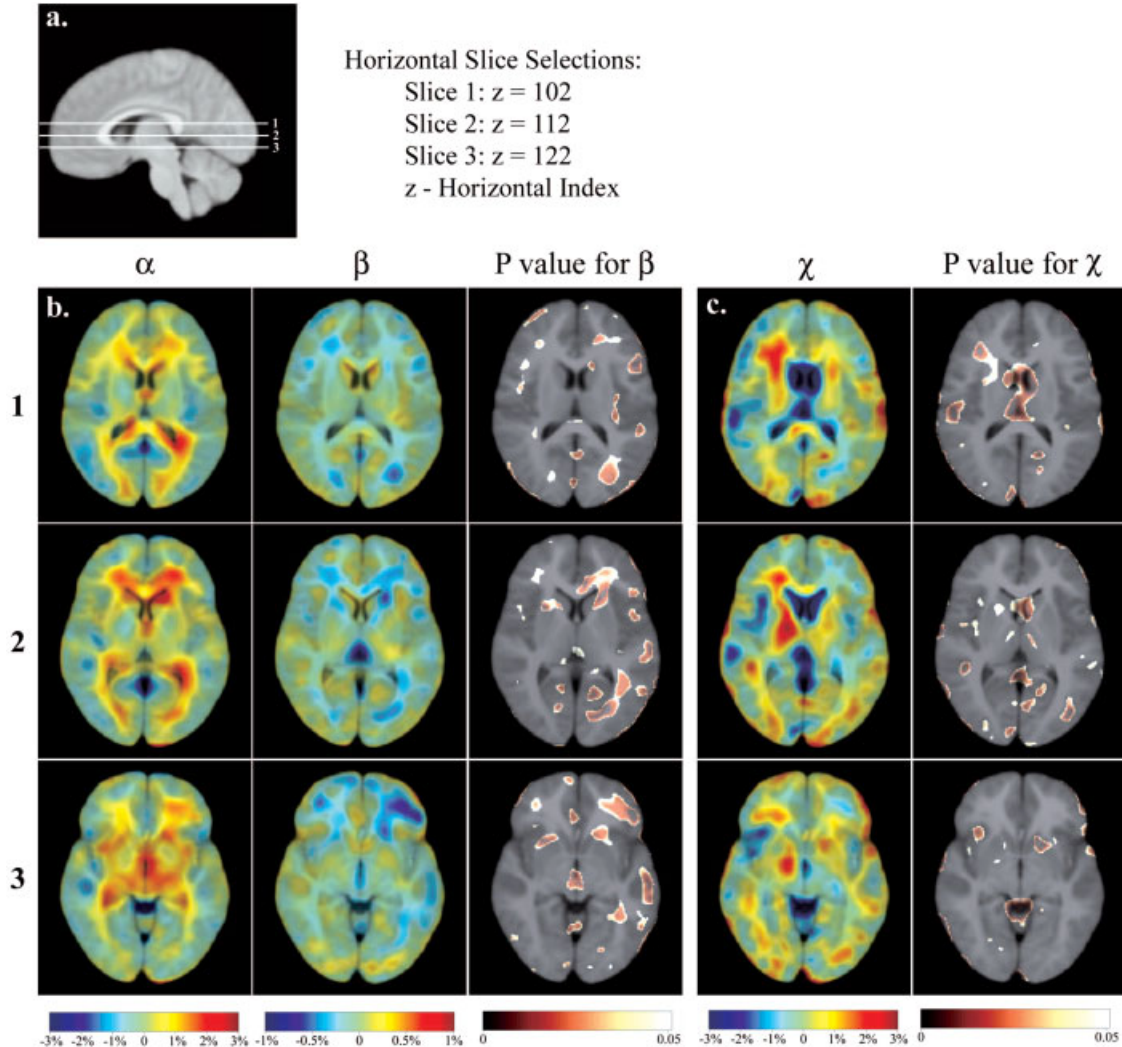


Figure 6.

Linear regression with age and gender. Panel (a) shows the MDT brain anatomy and the slice selections ($z = 102, 112, \text{ or } 122$). Panel (b) displays the result of linear regression with age. Model: annual tissue growth rate = $\beta \cdot (\text{age} - \text{mean age}) + \alpha$. The intercept α demonstrates a strong growth in white matter at the mean age of 12.3 years. The linear coefficient β and its P -value map from t -test ($P \leq 0.05$) depict the regions with changes in growth rate. The dark blue regions signify a deceleration in

growth rates. Panel (c) illustrates the result of linear regression with the added gender term. Model: annual tissue growth rate = $\beta \cdot (\text{age} - \text{mean age}) + (\chi \cdot \text{gender} + \alpha)$. The same slice selections as in panel (b) are used. Because the intercept α and age coefficient β remain similar while the gender term has been added, only the gender coefficient χ and its P -value map ($P \leq 0.05$) are displayed.

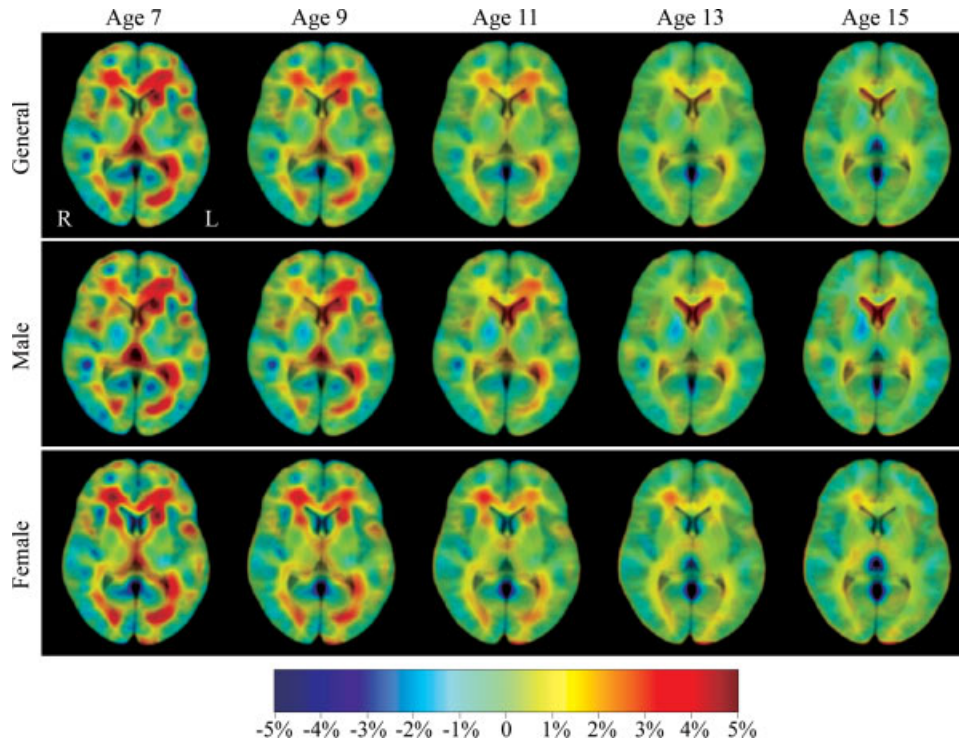


Figure 7.

Tissue growth maps modeled by linear regression. Top row displays the growth maps at different ages modeled with age-dependent linear regression as in Figure 6b. Bottom two rows show the gender specific growth maps over time modeled with both age and gender effects as shown in Figure 6b,c. The slice selection corresponds to the slice 2 in Figure 6.

ing P -values at the horizontal sections. The map of α demonstrates an extensive growth of white matter tract system at a rate of 1–3% annually, at the mean age of 12.3 years. The result from the linear coefficient β suggests a slowing down of the growth rate over time in regions with the greatest white matter growth. An age effect on gray matter shrinkage was also apparent, however, the effect is not large enough to reach statistical significance. We attempted to study the gender effect by adding an additional gender specific component (χ) for the intercept. The map of χ visualizes the spatial difference in growth patterns between the two genders. It is noteworthy that the regional growth at lateral ventricles and caudate nuclei is higher for boys than girls.

The overall significance of the age effect in the regression was estimated by permutation tests (ROI—the entire brain). The permutation P value for the negative correlation between age and Jacobian map is 0.0592. This value indicates the significance level of the trend, that growth rate is slowing down as age increases.

Growth Maps Recovered From Linear Regression

Finally, the mean growth maps at different ages were recovered by plotting the linear model with fitted correla-

tion coefficients (Fig. 7). The top row demonstrates the age effect in growth pattern changes, with strong white matter growth from age 7–9 years and less overall expansion at older ages. The bottom two rows exhibit the gender specific growth maps at different ages. We detected similar,

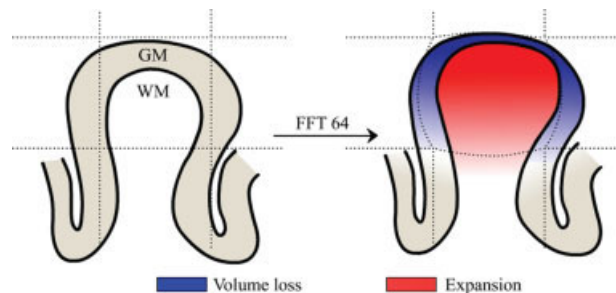


Figure 8.

Partial volume effect. A relatively large computational voxel (outlined by the dotted lines) could contain both gray matter (GM) and white matter (WM). The illustrated voxel holds a large proportion of growing white matter (red) with a small proportion of shrinking gray matter (blue), the overall signal from this voxel will be dominated by the white matter growth.

age-related white matter growth, and an uneven growth pattern between males and females.

DISCUSSION

TBM is a non-linear image registration tool that measures brain changes using serial MRI scans. The Jacobian determinants of the deformation map are used to provide 3D visualization of local tissue growth or atrophy with improved spatial resolution compared to traditional volumetry-based morphometry (VBM). We demonstrate this advantage in the individual study (Fig. 3). Visual inspection suggests a localized white matter growth in the orbito-frontal area. The overall increase in frontal white matter volume is 1%, as calculated by integrating the Jacobian determinants over the region-of-interest. This result is comparable to the large scale longitudinal MRI study [Giedd et al., 1999]. Thus, TBM offers equivalent information to VBM with superior spatial details, making it a favorable method for studying age and disease-related changes in brain morphometry.

Our results from the permutation tests confirm previous developmental MRI studies that have provided evidence for age-related increases in total white matter volume and decreases in total gray matter volume [Caviness et al., 1996; Giedd et al., 1996; Jernigan et al., 1991; Pfefferbaum et al., 1994; Reiss et al., 1996; Sowell et al., 1999a]. Moreover, we provide detailed spatial mapping of the developing brain by utilizing the Jacobian matrix field to encode local volume changes. We have attained high resolution 3D mapping of white matter growth and growth dynamics. The frontiers of the tissue growth correspond well with the anatomical boundaries of brain structures such as cerebral white matter, indicating the sensitivity and specificity of our mapping approach. Global enlargement of white matter is observed across all lobes indicating an overall growth of white matter tract system in the subjects. Every brain was edited carefully by trained raters to include only brain tissues. Nevertheless, there could still be a small amount of registration errors at the edge of the brain due to imperfect segmentation and/or registration. As a result, the brain masks (ROI) used in this study do not include boundary voxels. Therefore, the results of permutation tests provide accurate estimate of the overall significance levels within each region-of-interest.

Postmortem studies have revealed an extended myelination process that continues into the third decade of life, especially for frontal and parietal regions [Yakovlev and Lecours, 1967]. Several recent findings also suggest an accelerated maturation of gray and white matter in frontal lobe during adolescence [Giedd et al., 1999; Sowell et al., 1999b]. In this study, we demonstrate a wide-spread growth in white matter, with the most prominent expansion in the frontal lobe. Inference on white matter growth using TBM, however, is based on changes in tissue boundaries or gray/white contrast, which are related to the

underlying tissue microstructure. Nevertheless, it does not offer a direct measurement of the true changes to white matter integrity or myelination. MR spectroscopy [Lopez-Villegas et al., 1996] and quantitative MR relaxometry [House et al., 2006] might provide a better answer to address these questions.

The individual growth map shown in Figure 3 demonstrates cortical gray matter tissue growth over the primary sensorimotor areas. The same growth pattern is revealed again in the group average map (Fig. 5). However, other studies has shown gray matter loss in dorsal parietal and primary sensorimotor regions at this age range [Gogtay et al., 2004; Sowell et al., 2003]. This seemingly discrepant result might be explained by the partial volume effect. At the resolution of FFT 64, the size of each computational voxel is about 30 mm^3 ($199 \text{ mm}/64 = 3.1 \text{ mm}$). This is a relatively large size that might contain both gray and white matter within the same voxel, especially for the areas where the gray matter is thin. As illustrated in Figure 8, if the voxel holds a large proportion of growing white matter with a small proportion of shrinking gray matter, the overall signal from that voxel will be dominated by the white matter growth.

Our study is based on 13 developing children with two consecutive brain scans taken as they matured in age. The data set is relatively small compared to the few medium-to-large scale neuro-imaging studies published to date [Giedd et al., 1999; Paus et al., 1999; Sowell et al., 2004]. The warp diagram (Fig. 4) is implemented to compensate for this relatively low degree of freedom and large variance among individual brains. The step of inter-subject registration is computationally intensive but it matches the local shape properties among the subjects. This enables regional comparisons and voxel-wise statistical analyses of the growth maps. A larger sample size would further improve the power, and it is necessary to track the gender specific patterns in brain development.

In this study, we map the patterns of normal brain development using TBM. TBM is a highly automated image analysis technique that delineates local tissue gain or loss at a greater spatial resolution than the traditionally used volumetry-based method. In addition to brain development, TBM has a wide spectrum of applications in longitudinal brain analysis, such as understanding how brain is affected by certain psychiatric disorders (e.g. autism, schizophrenia, depression, etc), tracking degenerative disease progression, and monitoring drug treatment effect. In future work, we look to apply TBM to a study with relatively large sample size and expand the statistical models to answer interesting questions like brain asymmetry, correlations with IQ, cognitive measures, as well as genome types.

ACKNOWLEDGMENTS

Information on the National Centers for Biomedical Computing can be obtained from <<http://nihroadmap>>.

nih.gov/bioinformatics>. Contents are solely the responsibility of the authors and do not necessarily represent the official views of NCRR or NIH.

REFERENCES

- Ashburner J, Friston KJ (2003): Morphometry. In: Ashburner J, Friston KJ, Penny W, editors. *Human Brain Function*, 2nd ed. San Diego, CA: Academic Press. 707 p.
- Caviness VS Jr, Kennedy DN, Richelme C, Rademacher J, Filipek PA (1996): The human brain age 7–11 years: A volumetric analysis based on magnetic resonance images. *Cereb Cortex* 6:726–736.
- Chiang MC, Dutton RA, Hayashi KM, Lopez OL, Aizenstein HJ, Toga AW, Becker JT, Thompson PM (2007): 3D pattern of brain atrophy in HIV/AIDS visualized using tensor-based morphometry. *Neuroimage* 34:44–60.
- Chung MK, Worsley KJ, Paus T, Cherif C, Collins DL, Giedd JN, Rapoport JL, Evans AC (2001): A unified statistical approach to deformation-based morphometry. *Neuroimage* 14:595–606.
- Efron B, Tibshirani R (1993): *An Introduction to the Bootstrap*. London: Chapman & Hall.
- Efron B, Tibshirani R (1986): Bootstrap methods for standard errors, confidence intervals, and other measures of statistical accuracy. *Stat Sci* 1:54–77.
- Freeborough PA, Fox NC (1998): Modeling brain deformations in Alzheimer disease by fluid registration of serial 3D MR images. *J Comput Assist Tomogr* 22:838–843.
- Giedd JN, Snell JW, Lange N, Rajapakse JC, Casey BJ, Kozuch PL, Vaituzis AC, Vauss YC, Hamburger SD, Kaysen D, Rapoport JL (1996): Quantitative magnetic resonance imaging of human brain development: Ages 4–18. *Cereb Cortex* 6:551–560.
- Giedd JN, Blumenthal J, Jeffries NO, Castellanos FX, Liu H, Zijdenbos A, Paus T, Evans AC, Rapoport JL (1999): Brain development during childhood and adolescence: A longitudinal MRI study. *Nat Neurosci* 2:861–863.
- Gogtay N, Giedd JN, Lusk L, Hayashi KM, Greenstein D, Vaituzis AC, Nugent TF III, Herman DH, Clasen LS, Toga AW, et al. (2004): Dynamic mapping of human cortical development during childhood through early adulthood. *Proc Natl Acad Sci USA* 101:8174–8179.
- Good CD, Johnsrude IS, Ashburner J, Henson RN, Friston KJ, Frackowiak RS (2001): A voxel-based morphometric study of ageing in 465 normal adult human brains. *Neuroimage* 14(1, Part 1):21–36.
- Hand DJ, Crowder MJ (1996): *Practical Longitudinal Data Analysis*. London: Chapman & Hall. 232 p.
- House MJ, St Pierre TG, Foster JK, Martins RN, Clarnette R (2006): Quantitative MR imaging R2 relaxometry in elderly participants reporting memory loss. *AJNR Am J Neuroradiol* 27:430–439.
- Jernigan TL, Trauner DA, Hesselink JR, Tallal PA (1991): Maturation of human cerebrum observed in vivo during adolescence. *Brain* 114 (Part 5):2037–2049.
- Kaufman J, Birmaher B, Brent D, Rao U, Flynn C, Moreci P, Williamson D, Ryan N (1997): Schedule for affective disorders and schizophrenia for school-age children-present and lifetime version (K-SADS-PL): Initial reliability and validity data. *J Am Acad Child Adolesc Psychiatry* 36:980–988.
- Kochunov P, Lancaster J, Thompson P, Toga AW, Brewer P, Hardies J, Fox P (2002): An optimized individual target brain in the Talairach coordinate system. *Neuroimage* 17:922–927.
- Kochunov P, Lancaster J, Hardies J, Thompson PM, Woods RP, Cody JD, Hale DE, Laird A, Fox PT (2005): Mapping structural differences of the corpus callosum in individuals with 18q deletions using targetless regional spatial normalization. *Hum Brain Mapp* 24:325–331.
- Kovacevic N, Henderson JT, Chan E, Lifshitz N, Bishop J, Evans AC, Henkelman RM, Chen XJ (2005): A three-dimensional MRI atlas of the mouse brain with estimates of the average and variability. *Cereb Cortex* 15:639–645.
- Leow AD, Huang SC, Geng A, Becker JT, Davis SW, Toga AW, Thompson PM (2005a): Inverse consistent mapping in 3D deformable image registration: its construction and statistical properties. *Information Processing in Medical Imaging (IPMI)*, Glenwood Springs, Colorado, LNCS 2565, pp. 493–503.
- Leow AD, Klunder AD, Jack CR, Toga AW, Dale AM, Bernstein MA, Britson PJ, Gunter JL, Ward CP, Whitwell JL, et al. (2005b): Longitudinal stability of MRI for mapping brain change using tensor-based morphometry. *Neuroimage* 31:627–640.
- Lopez-Villegas D, Kimura H, Tunlayadechanont S, Lenkinski RE (1996): High spatial resolution MRI and proton MRS of human frontal cortex. *NMR Biomed* 9:297–304.
- MacDonald D (1993): <http://www.bic.mni.mcgill.ca/software/register/register.html>.
- Maes F, Collignon A, Vandermeulen D, Marchal G, Suetens P (1997): Multimodality image registration by maximization of mutual information. *IEEE Trans Med Imaging* 16:187–198.
- Mazziotta J, Toga A, Evans A, Fox P, Lancaster J, Zilles K, Woods R, Paus T, Simpson G, Pike B, et al. (2001): A probabilistic atlas and reference system for the human brain: International Consortium for Brain Mapping (ICBM). *Philos Trans R Soc Lond B Biol Sci* 356:1293–1322.
- Nichols TE, Holmes AP (2002): Nonparametric permutation tests for functional neuroimaging: A primer with examples. *Hum Brain Mapp* 15:1–25.
- Paus T, Zijdenbos A, Worsley K, Collins DL, Blumenthal J, Giedd JN, Rapoport JL, Evans AC (1999): Structural maturation of neural pathways in children and adolescents: In vivo study. *Science* 283:1908–1911.
- Pfefferbaum A, Mathalon DH, Sullivan EV, Rawles JM, Zipursky RB, Lim KO (1994): A quantitative magnetic resonance imaging study of changes in brain morphology from infancy to late adulthood. *Arch Neurol* 51:874–887.
- Reiss AL, Abrams MT, Singer HS, Ross JL, Denckla MB (1996): Brain development, gender and IQ in children. A volumetric imaging study. *Brain* 119 (Part 5):1763–1774.
- Rex DE, Ma JQ, Toga AW (2003): The LONI Pipeline Processing Environment. *Neuroimage* 19:1033–1048.
- Riddle WR, Li R, Fitzpatrick JM, DonLevy SC, Dawant BM, Price RR (2004): Characterizing changes in MR images with color-coded Jacobians. *Magn Reson Imaging* 22:769–777.
- Shattuck DW, Leahy RM (2002): BrainSuite: An automated cortical surface identification tool. *Med Image Anal* 6:129–142.
- Sled JG, Zijdenbos AP, Evans AC (1998): A nonparametric method for automatic correction of intensity nonuniformity in MRI data. *IEEE Trans Med Imaging* 17:87–97.
- Sowell ER, Thompson PM, Holmes CJ, Batth R, Jernigan TL, Toga AW (1999a): Localizing age-related changes in brain structure between childhood and adolescence using statistical parametric mapping. *Neuroimage* 9(6, Part 1):587–597.
- Sowell ER, Thompson PM, Holmes CJ, Jernigan TL, Toga AW (1999b): In vivo evidence for post-adolescent brain maturation in frontal and striatal regions. *Nat Neurosci* 2:859–861.

- Sowell ER, Peterson BS, Thompson PM, Welcome SE, Henkenius AL, Toga AW (2003): Mapping cortical change across the human life span. *Nat Neurosci* 6:309–315.
- Sowell ER, Thompson PM, Leonard CM, Welcome SE, Kan E, Toga AW (2004): Longitudinal mapping of cortical thickness and brain growth in normal children. *J Neurosci* 24:8223–231.
- Thompson PM, Giedd JN, Woods RP, MacDonald D, Evans AC, Toga AW (2000): Growth patterns in the developing brain detected by using continuum mechanical tensor maps. *Nature* 404:190–193.
- Thompson PM, Hayashi KM, de Zubicaray G, Janke AL, Rose SE, Semple J, Herman D, Hong MS, Dittmer SS, Doddrell DM, et al. (2003): Dynamics of gray matter loss in Alzheimer’s disease. *J Neurosci* 23:994–1005.
- Toga AW (1999): *Brain Warping*. San Diego, CA: Academic Press. 385 p.
- Wells WM III, Viola P, Atsumi H, Nakajima S, Kikinis R (1996): Multi-modal volume registration by maximization of mutual information. *Med Image Anal* 1:35–51.
- Woods RP, Grafton ST, Watson JD, Sicotte NL, Mazziotta JC (1998): Automated image registration. II. Intersubject validation of linear and nonlinear models. *J Comput Assist Tomogr* 22:153–165.
- Yakovlev PI, Lecours AR (1967): *The myelogenetic cycles of regional maturation of the brain*: Oxford: Blackwell.

APPENDIX: JACOBIAN MAPS

Detailed spatial and temporal mapping of brain structural changes is crucial to understanding the basis of age-related cognitive advancement and various brain disorders. TBM is an image analysis method based on non-linear registration. It identifies regional structural differences by examining the gradients of the deformation field. In general, it can be applied to detect any structural changes over time, such as during brain development and disease progression. It can also be used to map anatomical differ-

ences between different patient groups using cross-sectional data.

We explain here the application of TBM in the context of studying longitudinal brain changes. For each individual, serial MRI scans are acquired and TBM is applied to generate an individual Jacobian growth map, showing 3D profiles of tissue change over time. To formulate the process mathematically, we denote the follow-up scan as the source (S) and the baseline scan as the target (T). We compute a non-linear displacement vector field $u = (u_x, u_y, u_z)$ by deforming S to T using a mutual information (MI) based, inverse consistent mapping algorithm [Leow et al., 2005a]. Let $r = (x, y, z)$ denotes the voxel location. At satisfactory registration, $S(r - u)$ should correspond to $T(r)$ as their mutual information reaches maximum. The gradient of the deformation field, also called the Jacobian matrix field, is then used to quantify local changes. A 3D Jacobian deformation field is defined by:

$$J = \begin{pmatrix} \frac{\partial(x-u_x)}{\partial x} & \frac{\partial(y-u_y)}{\partial x} & \frac{\partial(z-u_z)}{\partial x} \\ \frac{\partial(x-u_x)}{\partial y} & \frac{\partial(y-u_y)}{\partial y} & \frac{\partial(z-u_z)}{\partial y} \\ \frac{\partial(x-u_x)}{\partial z} & \frac{\partial(y-u_y)}{\partial z} & \frac{\partial(z-u_z)}{\partial z} \end{pmatrix}$$

The determinant of the Jacobian matrix is derived from the forward deformation field. It is usually color coded to show regions of volume expansion $\det J(r) > 1$ or tissue shrinkage $\det J(r) < 1$ [Ashburner and Friston, 2003; Chung et al., 2001; Freeborough and Fox, 1998; Riddle et al., 2004; Thompson et al., 2000; Toga, 1999]. Once individual Jacobian maps have been created and spatially aligned to a standard coordinate system, statistical parametric maps are typically established to investigate various scientific questions such as localization of group difference, age and gender effect, correlation with disease severity, or complex interaction between effects of interest [Ashburner and Friston, 2003].